ARTICLE

Circular RNA profile identifies circOSBPL10 as an oncogenic factor and prognostic marker in gastric cancer

Sen Wang [1] · Xing Zhang[1] · Zheng Li[1] · Weizhi Wang[1] · Bowen Li[1] · Xiaoxu Huang[1] · Guangli Sun[1] · Jianghao Xu[1] · Qing Li[1] · Zhipeng Xu[1] · Yiwen Xia[1] · Lu Wang[1] · Qiang Zhang[1] · Qiang Li[1] · Lu Zhang[1] · Jie Chen[2] · Yangjun Wu[2] · Jiacheng Cao[1] · Penghui Xu[1] · Diancai Zhang[1] · Hao Xu[1] · Zekuan Xu [1,3]

Abstract

The prognosis after curative resection of gastric cancer (GC) remains unsatisfactory, and thus, the development of treatments involving alternative molecular and genetic targets is critical. Circular RNAs (circRNAs), which are newly discovered molecules with key roles in the non-coding RNA network, have been identified as critical regulators in various cancers. Here, we aimed to determine the circRNA expression profile and to investigate the functional and prognostic significance of circRNA in GC. Using next-generation sequencing profiling, we first characterized an abundant circRNA in GC, hsa_circ_0008549, derived from the OSBPL10 gene and named it circOSBPL10. The expression of circOSBPL10 was found to be upregulated in GC tissues by quantitative RT-PCR, and silencing of circOSBPL10 significantly inhibited GC cell growth, migration, and invasion in multiple experiments. We further confirmed that miR-136-5p is a downstream target of circOSBPL10 using RNA pull-down and luciferase reporter assays. Rescue experiments confirmed that circOSBPL10 regulates biological functions in GC cells via a circOSBPL10-miR-136-5p-*WNT2* axis. In vivo experiments showed that circOSBPL10 promotes tumor growth and metastasis in mice. Furthermore, the level of circOSBPL10 was observed to be a prognostic marker of the overall survival and disease-free survival of patients with GC. Taken together, our findings reveal that circOSBPL10 may serve as a new proliferation factor and prognostic marker in GC.

Introduction

Gastric cancer (GC) is one of the most common and malignant tumors, with a high recurrence rate and a poor 5-year survival rate [1]. It is the fourth most common cancer, the third leading cause of cancer-related death worldwide and ranked second in both most common cancers and cancer mortalities in China [2–4]. Surgical treatment, such as gastric resection and D2 lymph node dissection, is still the most frequently recommended treatment for GC patients [5]. However, the prognosis after surgery remains unsatisfactory [6]. Therefore, exploration of the underlying mechanisms, the development of treatments involving alternative molecular and genetic targets and the pursuit of prognostic markers are critical.

Circular RNA (circRNA), which is generated from back-splicing of precursor mRNA, is a special form of RNA with a circular instead of a linear structure that is found in eukaryotes [7–9]. circRNAs feature a closed loop without a free 3′ and 5′ end and, thus, are highly conserved and stable [10, 11]. circRNAs were first discovered > 20 years ago but were initially considered to be by-products of splicing errors and genomic junk [11–14]. Little attention was paid to circRNAs, but in recent years, the rapid development of next-generation sequencing-based profiling of non-coding RNAs in human cells and bioinformatics approaches has

✉ Zekuan Xu
  xuzekuan@njmu.edu.cn

1   Department of General Surgery, The First Affiliated Hospital of Nanjing Medical University, Nanjing, Jiangsu 210029, P. R. China

2   Fudan University Shanghai Cancer Center, Shanghai Medical College, Fudan University, Shanghai 200032, P. R. China

3   Collaborative Innovation Center For Cancer Personalized Medicine, Nanjing Medical University, Nanjing, Jiangsu 210029, P. R. China

changed how researchers view circRNAs [9, 15, 16]. Emerging evidence indicates that circRNAs participate in the progression of a variety of cancers, and several new circRNA targets have been identified [17–24]. In addition, circRNAs not only function in cancer but also in other diseases, such as neurological and cardiovascular diseases [9, 25–28].

In the current study, we adopted next-generation sequencing with circRNA and found that hsa_-circ_0008549 is upregulated in GC tissues. Herein, for the first time, we report that circOSBPL10 can promote cell proliferation and metastasis by sponging miR-136-5p, which was confirmed by multiple functional assays. A prognosis analysis indicated that circOSBPL10 could also serve as a valuable prognostic factor and a potential therapeutic target in future treatments.

Results

Profile of circRNAs in GC and normal tissues

Three GC tissue samples and their matched noncarcinoma adjacent tissues were collected for next-generation sequencing analysis. The flow chart is depicted in Fig. 1a. In total, 17,151 distinct circRNA candidates were identified, and 145 of these circRNAs were differentially expressed in cancerous tissues compared with matched noncancerous tissues. Among these differentially expressed circRNAs, 67 were upregulated and 78 were downregulated in GC tissues compared with noncancerous tissues (Fig. 1b). The raw data were submitted to the Gene Expression Omnibus database (GSE122796).

Characterization of circOSBPL10 in GC

Through next-generation sequencing (NGS) analysis, we identified the most differentially expressed circRNA (chr3:31917924-31921322, hsa_circ_0008549, termed circOSBPL10), which was derived from the OSBPL10 locus (Fig. 1b). The genomic structure shows that the second exon from the OSBPL10 gene is flanked by introns on each side, and the head-to-tail structure of circOSBPL10 was confirmed by Sanger sequencing using the BGC-823 cell line (Fig. 1c). Quantitative real-time RT-PCR (qRT-PCR) results confirmed that BGC-823 cells had the highest circOSBPL10 expression, followed by SGC-7901 cells (Fig. 1d). Therefore, we selected the BGC-823 and SGC-7901 cell lines for subsequent experiments throughout our study. RNase R exonuclease was added to the total RNA before reverse transcription. In both cell lines, the expression of mRNAs was decreased owing to digestion by RNase R (BGC-823, $P < 0.001$; SGC-7901, $P < 0.001$), whereas circular RNA levels did not decrease, indicating that they were

not affected by RNase R treatment (BGC-823: $P = 0.1811$; SGC-7901: $P = 0.0805$) (Fig. 1e). We conducted PCR using cDNA and gDNA (genomic DNA) treated with or without the RNase R in advance to detect the stability of circOSBPL10 (Fig. 1f). Under RNase R treatment, circOSBPL10 could resist digestion, whereas convergent primers could not amplify cDNA that was reverse-transcribed from mRNA. The results of PCR without RNase R treatment showed both amplification products that were reverse-transcribed using convergent and divergent primers from total RNA. No circRNA amplification products were observed using gDNA compared with cDNA. Next, we applied the transcription inhibitor actinomycin D in our experiments (Fig. 1g). Total RNA was extracted at the indicated time points (0, 4, 8, 12, and 24 h) followed by qRT-PCR. The results revealed that the transcript half-life of circOSBPL10 exceeded 24 h in both cell lines, whereas the linear transcript of OSBPL10 mRNA demonstrated a comparatively short half-time of < 4 h. Regarding localization, qRT-PCR analysis of nuclear and cytoplasmic RNA was performed after they were physically separated and fluorescence in situ hybridization (FISH) also showed that circOSBPL10 was preferentially localized within the cytoplasm (Fig. 1h, i). Taken together, our results demonstrate that circOSBPL10 is a stable cytoplasmic circRNA.

circOSBPL10 was significantly upregulated in GC tissues

The NGS profile revealed that circOSBPL10 is upregulated in GC tissues. qRT-PCR was performed in 70 paired primary cancer tissues and adjacent noncancerous tissues for validation. The expression levels of circOSBP10 were significantly higher in GC tissues than in noncancerous tissues ($P = 0.0118$, Fig. 2a). Among these paired samples, 63% ($n = 44$) exhibited higher expression in cancer tissues than in matched noncancerous tissues (Fig. 2b, c). The clinical pathological parameters of these patients are listed in Table 1. The expression in tumor tissues at T2–T4 was significantly higher than that at Tis-T1 ($P = 0.0111$) and in normal tissues ($P = 0.0016$), whereas expression in tumors at Tis-T1 did not differ from that in matched noncancerous tissues according to their T stage ($P = 0.1830$) (Fig. 2d). We then divided the tissues into I–II and III–IV stage tissues for further analysis and found that the expression of circOSBP10 in III–IV stage tissues was significantly higher than that in I–II stage tissues ($P = 0.0011$) and in noncancerous tissues ($P = 0.0002$). We also conducted an analysis of other clinical parameters, including gender, age, lymph node status, and location. The results revealed that the expression of circOSBPL10 was significantly higher in tumors located in the cardia than in non-cardia tumors (Supplementary Fig. S1a). No significant difference was
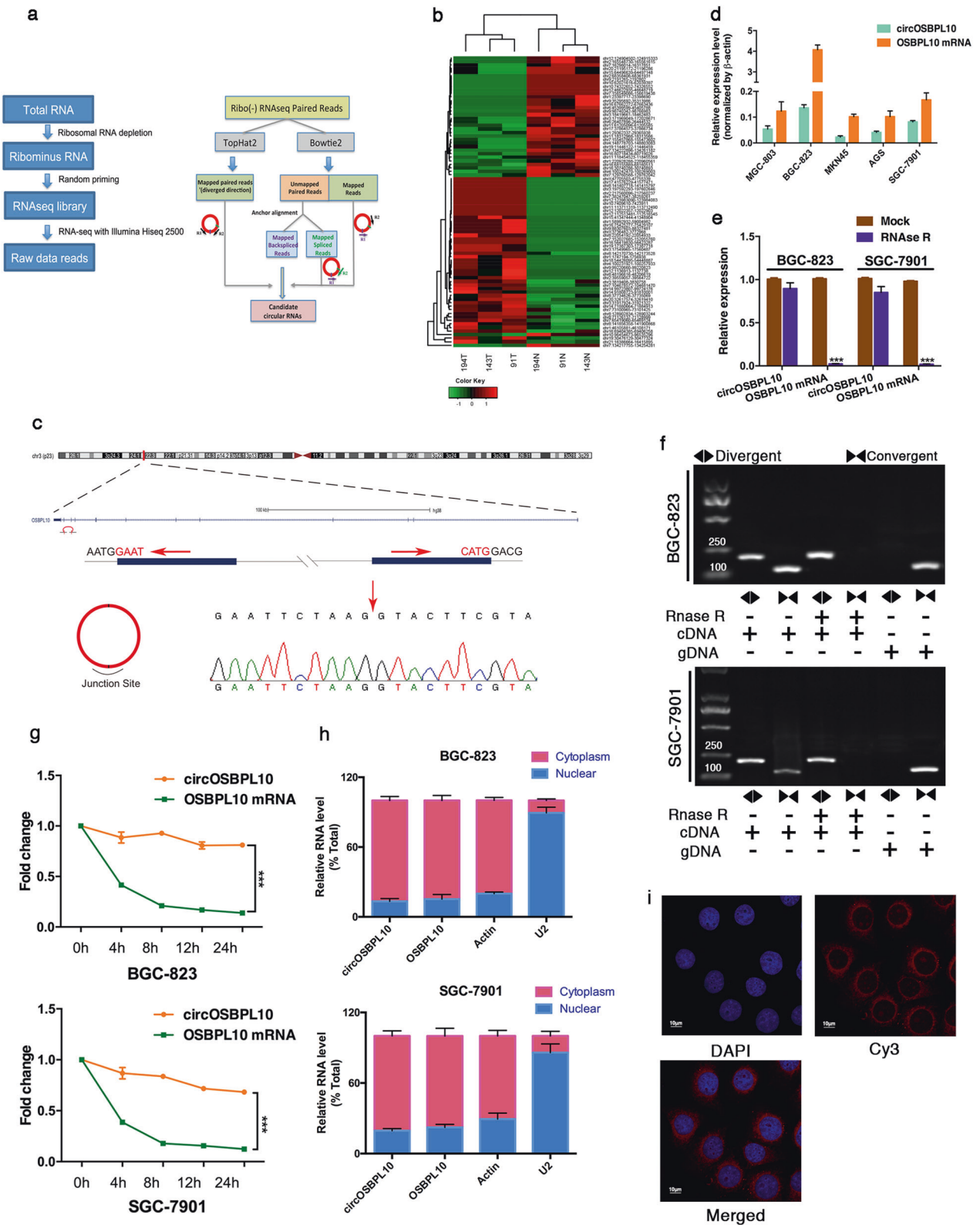
found for other parameters including age, gender, and lymph nodes status (Supplementary Fig. S1b–d). These results indicated that circOSBPL10 expression was markedly upregulated in GC tissues compared with matched noncancerous tissues and positively related to T and the tumor, node, metastasis (TNM) stage.

Fig. 1 Identification of circular RNAs by RNA-seq analyses in gastric cancer. **a** RNA-seq analysis of circular RNAs in three paired human gastric cancer tissues and matched noncancerous tissues. **b** Clustered heatmap of the differentially expressed circRNAs in three paired human gastric cancer tissues and matched noncancerous tissues. Rows represent circRNAs, whereas columns represent tissues. The circRNAs were classified according to the Pearson correlation. Red: upregulated, Green: downregulated. **c** Sanger sequencing-validated circular structure. Arrows indicate divergent primers that bind to genomic regions of circOSBPL10. **d** Expression levels of circOSBPL10 and OSBPL10 RNA validated by qRT-PCR were higher in BGC-823 and SGC-7901 cells among the five gastric cancer cell lines. **e** qRT-PCR analysis of circOSBPL10 and linear OSBPL10 abundance in BGC-823 and SGC-7901 gastric cell lines after RNase R treatment. **f** Linear and back-splicing products were amplified with convergent and divergent primers with and without treatment of RNase R and subjected to polymerase chain reaction. **g** qRT-PCR analysis of circOSBPL10 and OSBPL10 after treatment with actinomycin D at the indicated time points. **h** qRT-PCR analysis confirmed that circOSBPL10 and OSBPL10 are mainly located in the cytoplasm in BGC-823 and SGC-7901 cell lines. **i** RNA fluorescence in situ hybridization for circOSBPL10. Nuclei were stained with 4,6-diamidino-2-phenylindole (DAPI). Scale bar, 10 μm. The data represent the mean ± s.e.m. $^*P <$ 0.05, $^{**}P < 0.01$, $^{***}P < 0.001$

Silencing and overexpression of circOSBPL10 inhibits and promotes GC cell proliferation, invasion, and migration, respectively

To investigate the biological function of circOSBPL10, two siRNAs were designed to target the junction site (Supplementary Fig. S2a). A nonspecific siRNA sequence was used as the control. After cell transfection with siRNAs, the knockdown efficiencies of two siRNAs were confirmed by qRT-PCR (Supplementary Fig. S2b). As expected, the siRNAs directly suppressed the expression level of circOSBPL10 but did not affect the transcripts of linear OSBPL10 mRNA.

Next, we performed a 5-ethynyl-2′-deoxyuridine (EdU) incorporation assay to detect BGC-823 and SGC-7901 cell proliferation. After knockdown of circOSBPL10, the number of EdU + cells was significantly decreased compared with that in control cells (Fig. 3a). Both siRNAs also exerted significant antiproliferative effects compared with the control according to a CCK-8 proliferation assay (Supplementary Fig. S3a). Colony formation was also impaired after knockdown of circOSBPL10 in BGC-823 and SGC-7901 cells (Fig. 3b). Moreover, migration and invasion were significantly suppressed by the silencing of circOSBPL10 in both BGC-823 and SGC-7901 cell lines based on Transwell and impedance-based xCELLigence Real-Time Cell Analysis Detection Platform assays (Fig. 3, Supplementary Fig. S3b). We established a 3D GC organoid model to examine the proliferation competence of the tumor cells. The diameter of organoids transfected with the two siRNAs was dramatically decreased compared with the

diameter of control organoids (Fig. 3d). In addition, we also transfected overexpression vectors into both cell lines, and the efficiency was verified by qRT-PCR (Supplementary Fig. S2c). The results revealed that overexpression of circOSBPL10 significantly promoted the proliferation, migration and invasion of tumor cells (Supplementary Fig. S3c–f). Collectively, these findings suggest that circOSBPL10 is a key factor that affects the proliferation, migration, and invasion of GC cells.

circOSBPL10 serves as a miRNA sponge for miR-136-5P

We next explored the ability of circOSBPL10 to bind miRNAs. The online databases starbase, circNet, and RNA22 were used to predict potential target miRNAs of circOSBPL10. Among the predicted targets identified using these databases, we found 11 common miRNAs (miR-138-5p, miR-500b-3p, miR-151a-5p, miR-6879-3p, miR-1271a-5p, miR-449a, miR-125b-2-3p, miR-151b, miR-96-5p, mR-34a-5p, miR-136-5p) that could potentially be binding targets of circOSBPL10 (Fig. 4a). A biotin-labeled circOSBPL10 probe was designed and constructed to pull-down circOSBPL10 in two GC cell lines. The efficiency of the assay was first examined after pull-down, and the expression of circOSBPL10 was significantly enhanced in the circOSBPL10 transfectants, confirming that circOSBPL10 was successfully pulled down (Fig. 4b). We then detected the expression of candidate miRNAs using qRT-PCR after pull-down. In the BGC-823 group, significant increases in the expression of miR-500b-3p and miR-136-5p were observed among all 11 miRNA candidates, whereas in the SGC-7901 group, miR-6879-3p, miR-1271a-5p, miR-96a-5p, and miR-136-5p showed remarkably higher expression than other targets (Fig. 4c). Combining these two results, six miRNAs that could be potential targets in both GC cell lines emerged. Next, we constructed a circOSBPL10 luciferase reporter gene by inserting the circOSBPL10 fragments downstream of the luciferase reporter gene (LUC + circOSBPL10). HEK-293 cells were cotransfected with the luciferase reporters along with different RNA mimics. The luciferase activity assay indicated that among these targets, only miR-136-5p showed significantly decreased luciferase activity in HEK-293T cells (Fig. 4d). We then mutated the miRNA target site within the circOSBPL10 sequence in the 3′-UTR (Fig. 4e). No significant decrease was observed in the luciferase activity in the mutated miR-136-5p group (Fig. 4f). These results confirmed that miR-136-5p, but not other miRNA targets, could directly bind to circOSBPL10. In addition, we conducted a FISH assay to detect colocalization of circOSBPL10 (Cy3) and miR-136-5p (Fam) and found that they were mainly colocalized in the cytoplasm, further suggesting their interaction (Fig. 4g). Collectively, these results confirmed that

Fig. 2 circOSBPL10 is upregulated in gastric cancer and associated with clinical parameters. **a** qRT-PCR analysis in 70 paired gastric cancerous and noncancerous sample revealed that circOSBPL10 is upregulated in cancerous samples. **b** Percentage of upregulation and downregulation in paired tissue samples. **c** The fold changes (log10) of circOSBPL10 in each paired sample are arranged from high to low. **d** The association of circOSBPL10 expression and T stage through qRT-PCR. **e** The association of circOSBPL10 expression and TNM stage. The data represent the mean ± s.e.m. *$P < 0.05$, **$P < 0.01$, ***$P < 0.001$
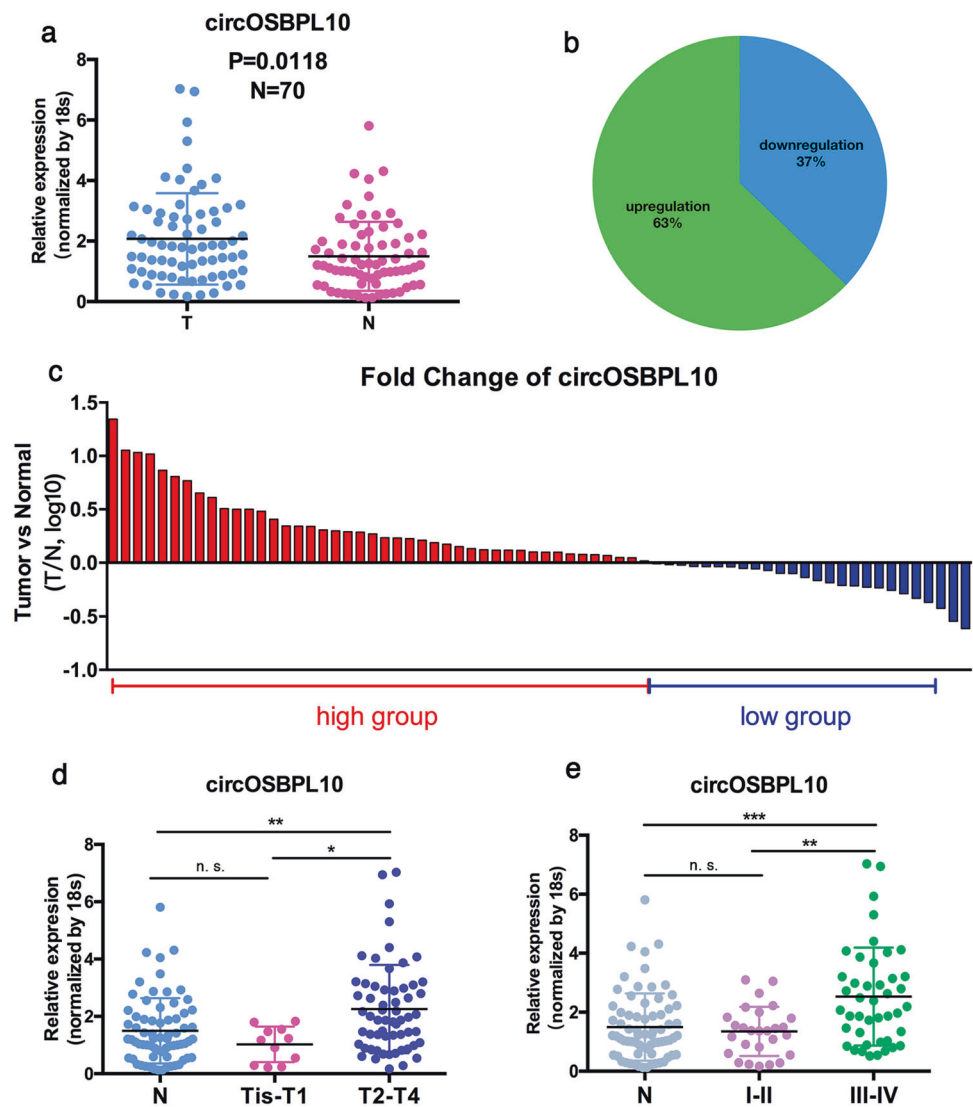

Table 1 Clinical parameters of 70 samples for circOSBPL10 and miR-136-5p

circOSBPL10

| Parameters	Group	Cases	Expression of circOSBPL10	P value
Gender	Male	53	2.071 ± 0.2206 $N = 53$	$P = 0.9782$
	Female	17	2.083 ± 0.2896 $N = 17$	
Age	≥ 60	48	1.922 ± 0.1984 $N = 48$	$P = 0.2139$
	< 60	22	2.407 ± 0.3740 $N = 22$	
T stage	Tis-T1	11	1.024 ± 0.1866 $N = 11$	$P = 0.0111$
	T2–T4	59	2.257 ± 0.1984 $N = 59$	
Lymph code status	Negative	26	2.046 ± 0.3212 $N = 26$	$P = 0.8777$
	Positive	44	2.105 ± 0.2232 $N = 44$	
TNM stage	I–II	27	1.350 ± 0.1599 $N = 27$	$P = 0.0011$
	III–IV	43	2.529 ± 0.2534 $N = 43$	
Location	Cardia	18	2.993 ± 0.5072 $N = 18$	$P = 0.0021$
	Non-cardia	52	1.756 ± 0.1476 $N = 52$	
Total		70		
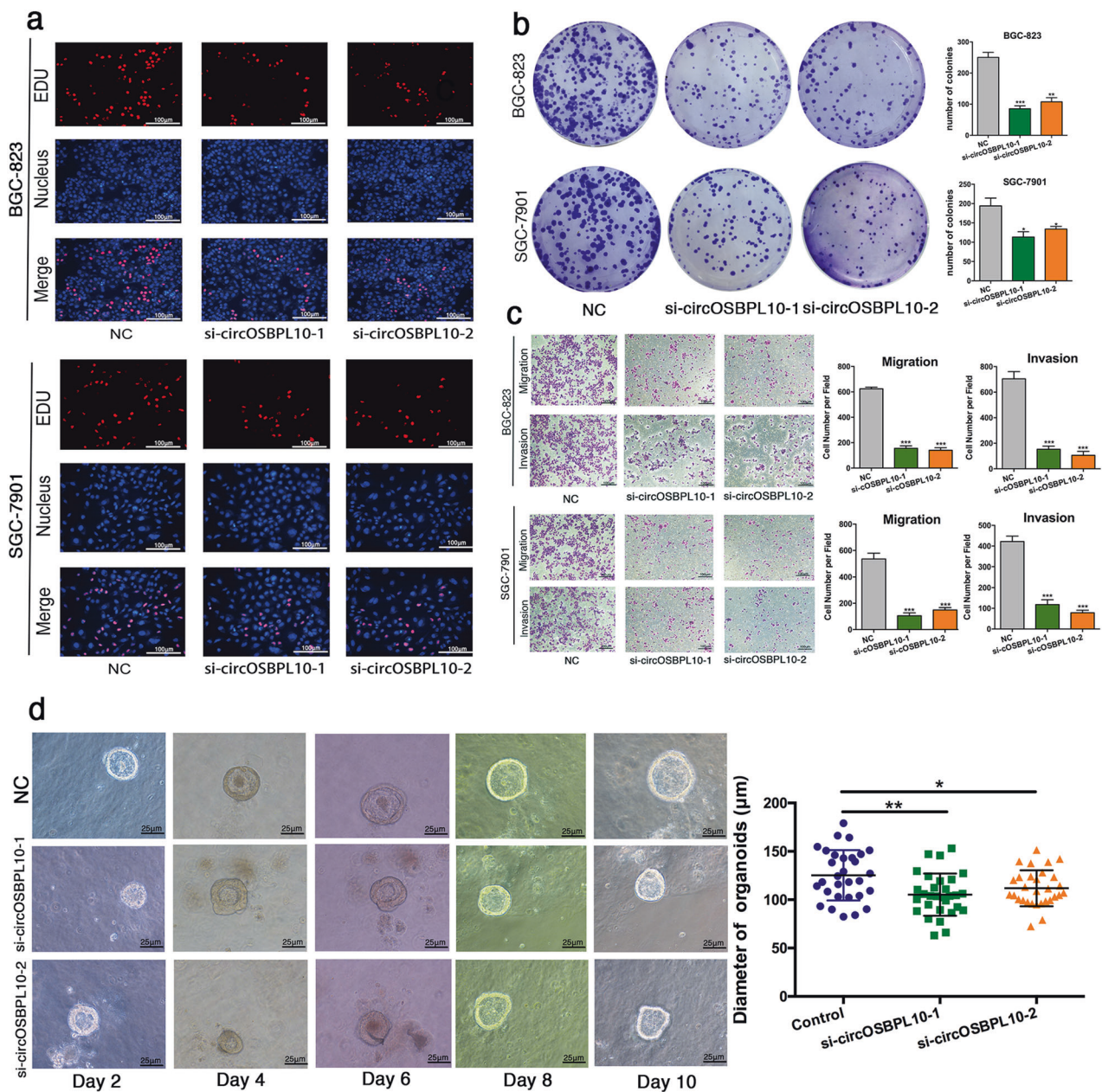
Fig. 3 Silencing of circOSBPL10 inhibits the proliferation of gastric cancer cells and suppresses gastric cancer cell migration and invasion. **a** Assessment of DNA synthesis using an EdU (5-ethynyl-2′-deoxyuridine) assay in BGC-823 and SGC-7901 cells transfected with control or circOSBPL10 siRNAs. Micrographs represent at least three experiments. Scale bar, 100 μm. **b** Colony formation assay of BGC-823 and SGC-7901 cells transfected with control or circOSBPL10 siRNAs. **c** Transfection of circOSBPL10 siRNAs suppressed the migration and invasion of BGC-823 and SGC-7901 cells. Scale bar, 100 μm. **d** Transfection of circOSBPL10 siRNAs suppressed gastric cancer organoid culture. The data represent the mean ± s.e.m. $^{*}P < 0.05$, $^{**}P < 0.01$, $^{***}P < 0.001$. Scale bar, 25 μm

circOSBPL10 binds to miR-136-5p in the cytoplasm and serves as a miRNA sponge for miR-136-5p.

The downstream circOSBPL10 target miR-136-5p promotes malignant biological functions by directly targeting WNT2 in vitro

After finding that miR-136-5p could be sponged by circOSBPL10, we investigated the downstream target of miR-136-5p to explore the pathogenic mechanisms of circOSBPL10. We first detected the expression of miR-136-5p in the same 70 paired tissues using qRT-PCR, and the clinical parameters are listed in Table 1. The expression level of miR-136-5p was significantly lower in cancerous samples than in paired noncancerous tissues ($P = 0.0107$). The associations between miR-136-5p expression and clinical parameters, including age, gender, lymph node status, location, and T stage, were also evaluated, but no
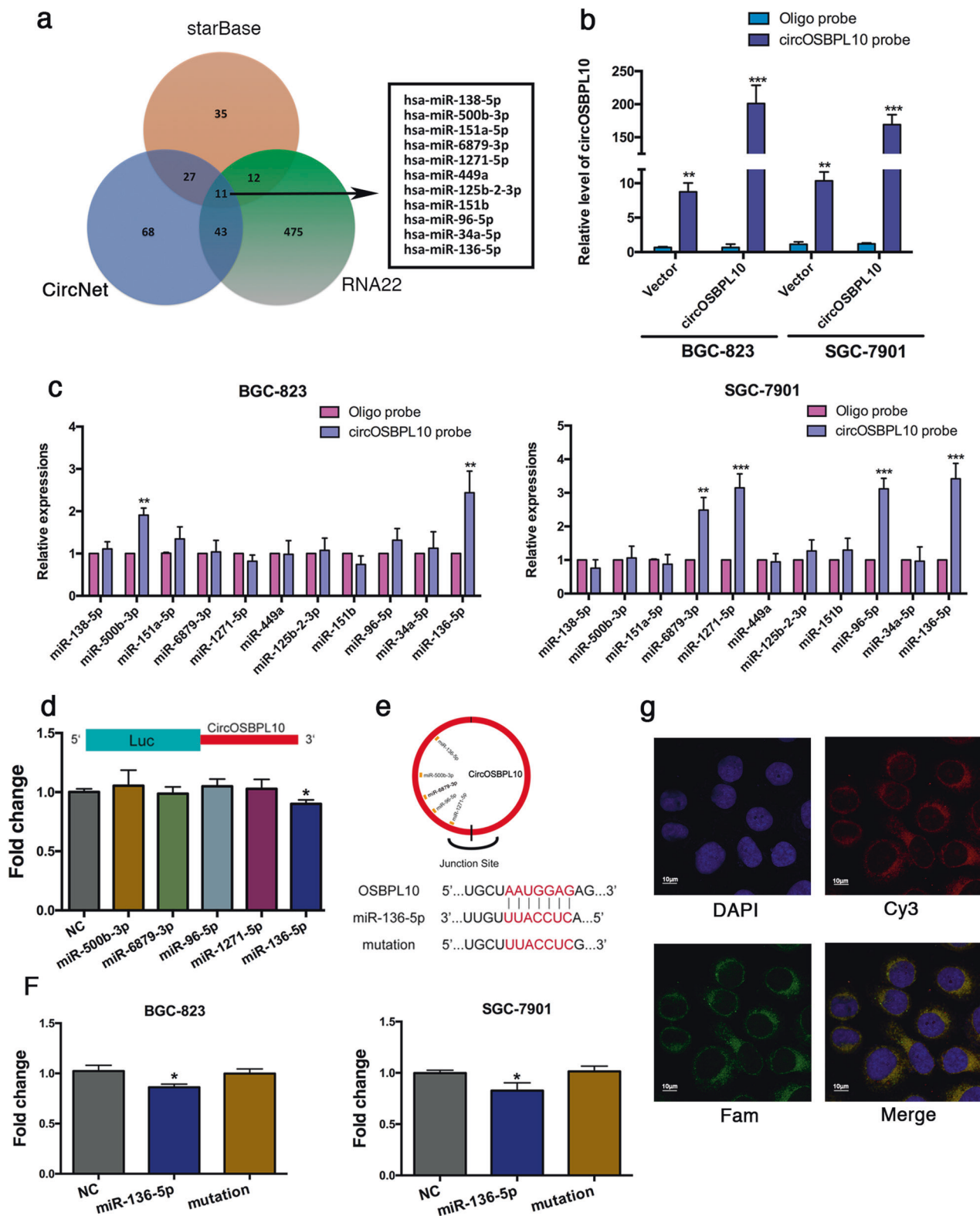
significant differences were found (Supplementary Fig. S4). In addition, the expression of miR-136-5p was remarkably higher in the normal gastric epithelium cell line GES-1 than in the BGC-823 and SGC-7901 cell lines (Fig. 5b). These results suggested that miR-136-5p is a tumor suppressor gene in GC, but how it exerts its function remains unknown.

The online database TargetScan was then used to predict the potential binding target of miR-136-5p. Among the

Fig. 4 circOSBPL10 serves as a sponge of miR-136-5p. **a** Venn diagram showing the overlap of target miRNAs of circOSBPL10 predicted by sttaBase, CircNet, and RNA22. **b** Lysates prepared from BGC-823 and SGC-7901 cells transfected with circOSBPL10 or vector were subject to RNA pull-down, and the efficiency was confirmed by qRT-PCR in BGC-823 and SGC-7901 cells. **c** Five target miRNAs in two cell lines were pulled down and confirmed by qRT-PCR. **d** A luciferase reporter assay was used to detect the luciferase activity of LUC-circOSBPL10 in HEK-293T cells transfected with mimics of the above miRNAs. The luciferase activity of miR-136-5p significantly decreased. **e** A schematic drawing shows the putative binding sites of miR-136-5p with circOSBPL10. **f** The luciferase activity of the LUC-circOSBPL10 or the LUC-circOSBPL10-mutant in both cells co-transfected with miRNA mimics was detected. **g** FISH revealed that circOSBPL10 and miR-136-5p were colocalized in the cytoplasm in BGC-823 cells. The circOSBPL10 probes were labeled with Cy3, and the miR-136-5p probes were labeled with Fam. The data represent the mean ± s.e.m. $^*P < 0.05$, $^{**}P < 0.01$, $^{***}P < 0.001$. Scale bar, 10 µm

potential targets, WNT2 was found to be a high-score target (Fig. 5c). In addition, a previous study confirmed that miR-136-5p could negatively regulate the expression of WNT2 [29]. Several studies have reported that WNT2 participates in the progression of gastrointestinal cancers [30–36]. Therefore, we hypothesized that WNT2 may be involved in the carcinogenesis process of the circOSBPL10-miR-136-5p axis and contribute to malignant behaviors. A luciferase reporter assay confirmed that Vector-WNT2-3′UTR combined with a miR-136-5p mimic significantly reduced luciferase activity ($P = 0.0076$), whereas co-transfection of cells with Vector-WNT2-3′UTR mut and the miR-136-5p mimic did not have a significant effect on luciferase activity. In both cell lines, the mRNA level of WNT2 decreased significantly after treatment of cells with the miR-136-5p mimic and increased after treatment with a miR-136-5p inhibitor, suggesting that WNT2 is negatively regulated by miR-136-5p at the transcriptional level (Fig. 5e). Cell migration and invasion ability determined by Transwell assays were both significantly inhibited after transfection of BGC-823 and SGC-7901 cells with miR-136-5p mimic (Fig. 5f). A colony formation assay revealed that the colony formation capability was also remarkably reduced in the miR-136-5p-treated group compared with the mimic NC group in both cell lines (Fig. 5g). The results above confirmed that miR-136-5p can negatively regulate malignant biological functions in GC cells, and thus, miR-136-5p emerged as a tumor suppressor gene.

Overexpression of circOSBPL10 rescued WNT2 expression and the enhanced proliferation, migration, and invasion induced by miR-136-5p

Next, we performed rescue experiments to determine whether circOSBPL10 promoted malignant biological functions in GC cell lines through the circOSBPL10-miR-136-5p-WNT2 axis. First, immunohistochemistry (IHC) confirmed that WNT2 is overexpressed in human GC tissue compared with paired noncancerous tissue, which was consistent with the previous experiments (Fig. 6a). qRT-PCR was also performed on 70 paired tissues to detect the mRNA expression of WNT2. We found that the expression of WNT2 was higher in tumor tissues than in paired noncancerous tissues (Supplementary Fig. S5a). Linear correlation analyses between circOSBPL10 and either miR-136-5p or WNT2 were performed separately. It turned out that circOSBPL10 was negatively correlated with miR-136-5p ($P = 0.0391$, $R^2 = 0.06110$, Supplementary Fig. S5b) and positively correlated with WNT2 ($P = 0.0003$, $R^2 = 0.1746$, Supplementary Fig. S5c), which strongly suggests involvement of the circOSBPL10-miR-136-5p-WNT2 axis. Unfortunately, the linear correlation analysis of miR-136-5p and WNT2 did not reach statistical significance ($P = 0.1921$, $R^2 = 0.02527$, Supplementary Fig. S5d). However, we believe that statistical significance would be reached if the sample size were increased. Next, to further elucidate this axis, BGC-823 and SGC-7901 cell lines were co-transfected with the miR-136-5p mimic and circOSBPL10 overexpression vector, and the protein expression of WNT2 was detected. Western blot confirmed that after treatment with miR-136-5p mimic, the protein expression levels of WNT2, phosphor β-catenin, and one of the classical downstream targets, matrix metalloproteinase-9 (MMP9), were significantly downregulated compared with the levels in controls. This protein expression could be rescued by overexpression of circOSBPL10, indicating that the Wnt/β-catenin pathway was activated by overexpression of circOSBPL10. The inhibitory effect on E-Cadherin expression was decreased by overexpression of miR-136-5p and rescued by ectopic expression of circOSBPL10, whereas, in contrast, Vimentin was inhibited by miR-136-5p (Fig. 6b). This finding confirmed that the Wnt/β-catenin pathway was activated and regulated by the circOSBPL10-miR-136-5p axis.

EdU and colony formation assays revealed that miR-136-5p mimic alone could significantly decrease cell growth. This effect could be rescued by cot-ransfection with miR-136-5p mimic and circOSBPL10 overexpression vector in both GC cell lines, confirming that the proliferation ability was regulated by the circOSBPL10-miR-136-5p axis (Fig. 6c, d). In addition, CCK-8 assays were conducted, and the results were consistent with the outcomes described above (Fig. 6e). Migration and invasion were examined using Transwell assays, which showed a significant reduction in miR-136-5p mimic-treated cells compared with control cells, whereas co-transfection with miR-136-5p mimic and circOSBPL10 overexpression vector increased the migration
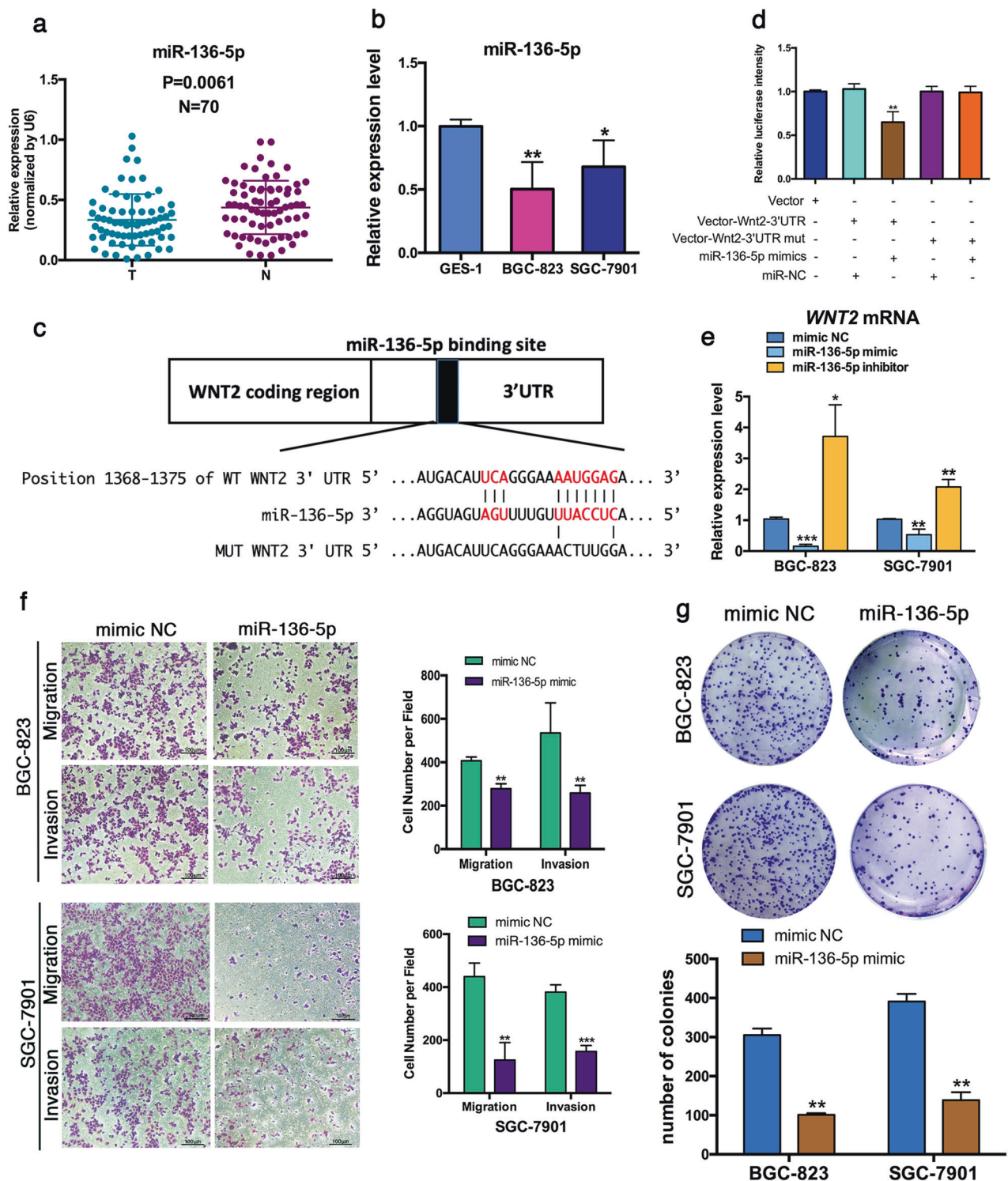
Fig. 5 miR-136-5p could serve as a tumor suppressor in gastric cancer. **a** qRT-PCR analysis in 70 paired cancerous and noncancerous tissues; miR-136-5p was significantly downregulated in gastric cancer tissue samples. **b** qRT-PCR analysis in cell lines confirmed that miR-136-5p was downregulated in BGC-823 and SGC-7901 cells compared with GES-1 cells. **c** The putative-binding site of miR-136-5p with *WNT2* and Mut sequence of *WNT2* predicted by TargetScan. **d** A luciferase reporter assay was used to detect the binding of miR-136-5p with *WNT2*-3′UTR and Mut-*WNT2*-3′UTR. **e** qRT-PCR analysis on *WNT2* treated with miR-136-5p mimics or miR-136-5p inhibitor in both BGC-823 and SGC-7901 cells. **f** Transwell assays indicated that miR-136-5p mimics suppressed migration and invasion of BGC-823 and SGC-7901 cells. Scale bar, 100 μm. **g** Colony formation assay on BGC-823 and SGC-7901 cells transfected with miR-136-5p mimics or inhibitor. The data represent the mean ± s.e.m. $^*P < 0.05$, $^{**}P < 0.01$, $^{***}P < 0.001$
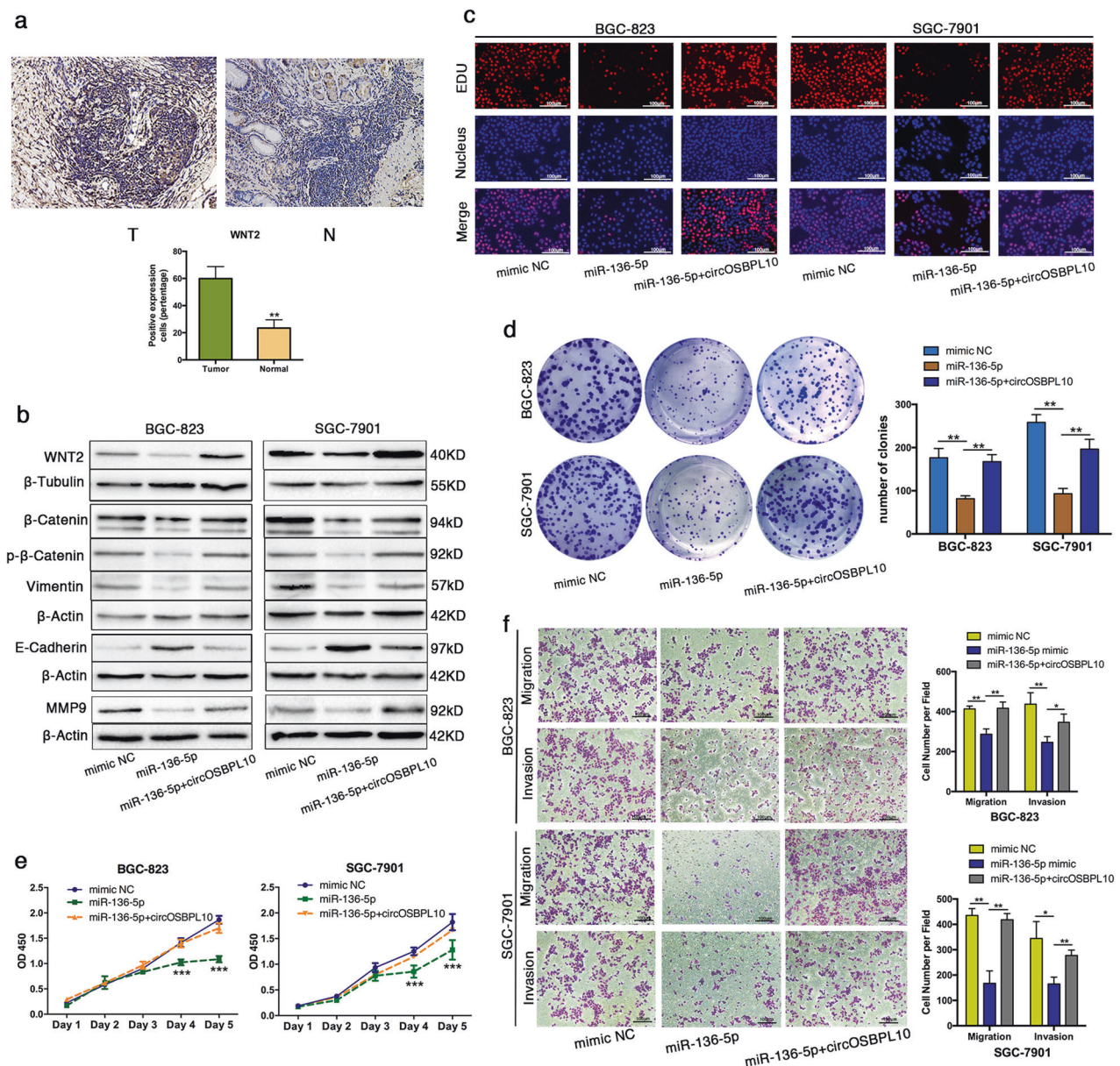
Fig. 6 Overexpression of circOSBPL10 reversed WNT2 expression, proliferation, migration, and invasion, which were inhibited by miR-136-5p. **a** Immunohistochemistry (IHC) analysis of WNT2 in gastric cancer tumor tissues and paired noncancerous tissues. **b** Western blot analysis of WNT2, total and phosphor β-catenin, Vimentin, E-Cadherin, and MMP9 with proteins treated with miR-136-5p mimics and circOSBPL10 overexpression plasmids in both cell lines. **c** EdU assay in BGC-823 and SGC-7901 cells transfected with control vector, miR-136-5p mimics, or circOSBPL10 overexpression plasmids. Scale bar, 100 μm. **d** Colony formation assay of BGC-823 and SGC-7901 transfected with control vector, miR-136-5p mimics or circOSBPL10 overexpression plasmids. **e** Assessment of proliferation of BGC-823 and SGC-7901 cells transfected with control vector, miR-136-5p mimics, or circOSBPL10 overexpression plasmids by CCK-8. **f** Transwell assays of BGC-823 and SGC-7901 cells transfected with control vector, miR-136-5p mimics or circOSBPL10 overexpression plasmids. The data represent the mean ± s.e.m. $^{*}P < 0.05$, $^{**}P < 0.01$, $^{***}P < 0.001$. Scale bar, 100 μm

and invasion ability compared with miR-136-5p mimic-treated cells (Fig. 6f). Collectively, these results suggested that overexpression of circOSBPL10 promoted proliferation, migration, and invasion through sponging of miR-136-5p and subsequently increasing the expression of WNT2, thereby leading to GC progression.

Overexpression and inhibition of circOSBPL10 in GC cell lines influences tumor growth and metastasis in vivo

We further evaluated the effects of overexpression and inhibition of circOSBPL10 in mouse models. Thirty-six
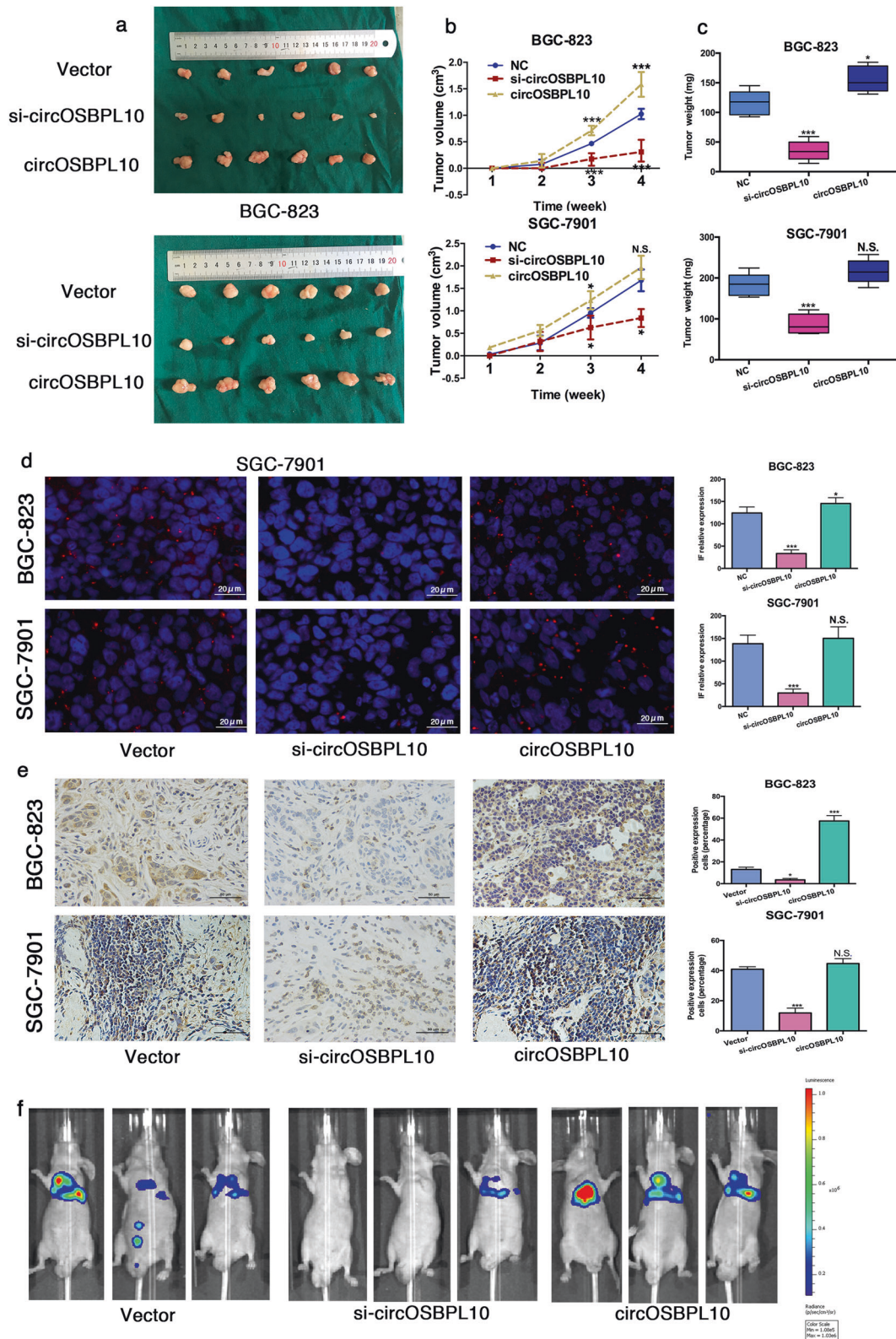
mice were assigned randomly to three groups to construct xenograft tumor models. After 4 weeks, all the mice in the three groups were sacrificed for examination. Tumors were measured throughout the experiment and weighed separately (Fig. 7a). Significantly decreased tumor volume was observed in the si-circOSBPL10 group for both cell lines

Fig. 7 Overexpression and inhibition of gastric cancer cell lines influence tumor growth and metastases in vivo. **a** Nude Balb/c mice ($n = 36$) were subcutaneously injected with BGC-823 and SGC-7901 cells (5×10^6 per mouse) transfected with control vector, cholesterol-modified siRNA or overexpression plasmids. **b** Tumor volumes were measured weekly in all mice that received subcutaneous injections. **c** After killing, tumors were extracted and weighed separately. **d** Immunofluorescence staining of WNT2 in resected tumor tissue. Scale bar: 20 μm. **e** Immunohistochemistry staining of WNT2 in resected tumor tissue. Scale bar: 50 μm **f** BGC-823 (5×10^6 cells/mL) transfected with control vector, cholesterol-modified siRNA or overexpression plasmids were injected into mice via the tail vein. Lung metastases were monitored and measured by luminescence. The data represent the mean ± s.e.m. $^*P < 0.05$, $^{**}P < 0.01$, $^{***}P < 0.001$

(Fig. 7b). A significant increase in tumor volume was also demonstrated in the lenti-circOSBPL10-overexpression group (circOSBPL10 group) in BGC-823 cells, whereas no significant difference in tumor volume emerged between the vector group and the circOSBPL10 group in SGC-7901 cells. Significantly reduced tumor weights in mice of the si-circOSBPL10 group were observed for both cell lines. Injection of lenti-circOSBPL10-overexpressing BGC-823 cells into mice resulted in significantly increased tumor weights, whereas no significant difference was found in mice injected with SGC-7901 cells (Fig. 7c). Significantly less-secreted WNT2 was observed via immunofluorescence (IF) and IHC in tumor sections from si-circOSBPL10 mice than in the tumors derived from injected cells with transfected with the vector (Fig. 7d, e). Overexpression of circOSBPL10 promoted WNT2 protein expression in the BGC-823 cell line according to IF and IHC. However, no significant difference in WNT2 expression was observed between the control and circOSBPL10 groups for the SGC-7901 cell line, which was consistent with previous results. Western blot was performed on the tumor tissues obtained from mice. Knockdown of circOSBPL10 inhibited the expression of phosphor β-catenin, Vimentin, MMP9, and increased the expression of E-Cadherin in tumors, whereas in the contrast, overexpression of circOSBPL10 increased phosphor beta-catenin, Vimentin, MMP9, and decreased E-Cadherin, respectively (Supplementary Fig. S6a).

Twelve mice were randomly divided into three groups for in vivo imaging to detect metastases using the BGC-823 cell line. Nine out of twelve mice survived after 4 weeks of observation. Knockdown of circOSBPL10 was found to significantly inhibit metastasis to the lung compared with the control, while overexpression of circOSBPL10 led to an increased number of lung metastases relative to the control. This result indicates that circOSBPL10 is a potential factor that promotes migration, which was consistent with the invasion and migration outcomes in GC cell lines (Fig. 7f). Hemotoxylin and eosin staining was performed to confirm the formation of lung metastases (Supplementary Fig. S6).

The prognostic value of circOSBPL10 in GC

To further investigate the prognostic value of circOSBPL10 in GC patients, overall survival (OS), and disease-free survival (DFS) curves were plotted using the Kaplan–Meier method. A total of 70 GC patients were followed up, and the patients were divided into two groups. The patients with a circOSBPL10 expression level in tumor that was higher than the mean of all patients were allocated to the circOSBPL10 (high) group ($n = 28$), whereas those with a circOSBPL10 expression level lower than the mean were allocated to the circOSBPL10 (low) group ($n = 42$). The results demonstrated that patients with a higher expression level of circOSBPL10 had significantly worse OS ($P = 0.0042$, Fig. 8a) and DFS ($P = 0.0013$, Fig. 8b) than those with the low levels of circOSBPL10. Moreover, to investigate the prognostic value of *WNT2* in GC, Kaplan–Meier plots were constructed through the kmplot website (http://kmplot.com/analysis/index.php?p = service), which is based on The Cancer Genome Atlas (TCGA) database. In both OS and DFS plots, patients with a lower *WNT2* expression level had significantly better survival than those with a higher *WNT2* expression level ($n = 876$, $P = 0.0078$, Fig. 8c; $n = 641$, $P = 0.0019$, Fig. 8d). These results further indicated that circOSBPL10 could serve as a prognostic factor in GC and that *WNT2* is also associated with poor survival. We also performed a survival analysis for miR-136-5p, but no significant difference was demonstrated, indicating that this miRNA is not a good target for GC prognosis (Supplementary Fig. S7)

Discussion

In this study, the circRNA profiles of GC and normal tissues confirmed that most circRNAs are of low abundance without statistical significance, possibly suggesting that these circRNAs are "junk" mRNA derived from splicing errors [9, 12, 37]. However, certain circRNAs are highly abundant in GC tissues according to NGS profiling. Therefore, we characterized for the first time one of the most differentially expressed circRNAs, circOSBPL10, and provide evidence that this circRNA may play a critical role in GC. To the best of our knowledge, this is the first study to report that the circular structure of OSBPL10 can promote GC. According to previous reports, linear OSBPL10 is not only linked with lipid metabolism but can also serve as an oncogene or a mutation target in prostate cancer, breast cancer, and lymphoma [38–43], possibly indicating that general underlying connections might exist behind the two forms. We confirmed the higher expression of circOSBPL10 in GC tissues and its positive correlation with T stage and TNM stage. Interestingly, circOSBPL10 was also

Fig. 8 circOSBPL10 is an independent prognostic marker of survival in patients with gastric cancer. **a** and **b** Kaplan–Meier analysis of the correlation between circOSBPL10 expression and overall survival (OS, **a**) and disease-free survival (DFS, **b**) in 70 patients with gastric cancer. Log-rank tests were used to determine statistical significance. **c** and **d** Kaplan–Meier analysis of the correlation between *WNT2* expression and overall survival (OS, **c**) and progression-free survival (PFS, **d**) in 876 and 641 patients, respectively, using the kmplot website based on TCGA database
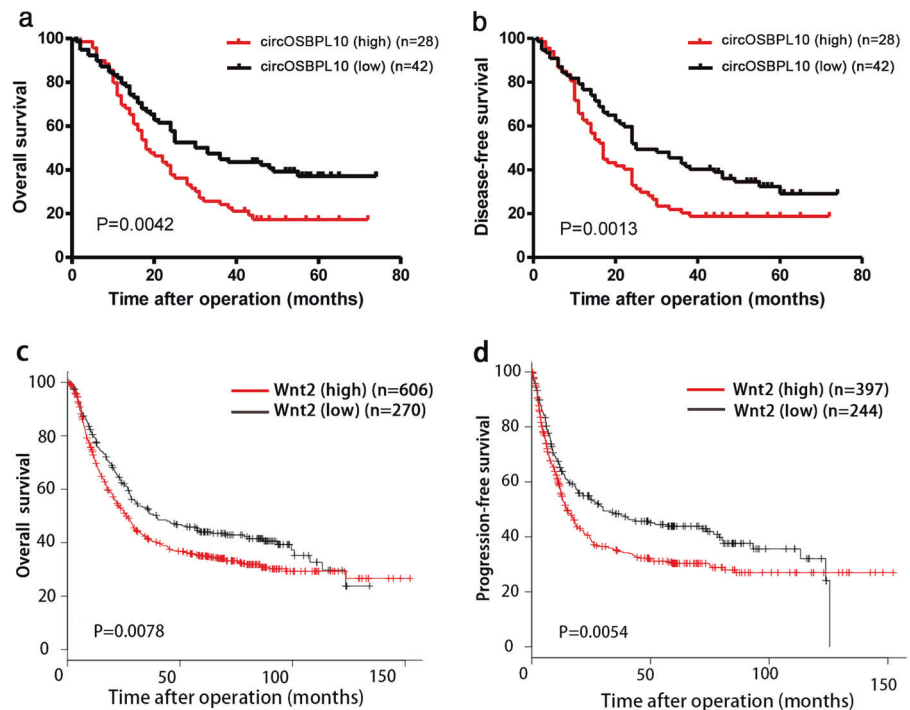
correlated with tumor location. It has been reported that the pathological features of GC located at the cardia and other gastric regions are different, and the screening ratio for early GC is comparatively lower at the cardia. This observation indicates that carcinogenesis at the cardia is unique and could possibly be related to circOSBPL10, although further confirmation is required.

It has been reported that circRNAs exert their function by acting as miRNA sponges, RNA-binding proteins, or transcription regulators. Moreover, few circRNAs can be translated into functional proteins/peptides [16]. Our results confirmed that circOSBPL10 could serve as a sponge of miR-136-5p, therefore forming a circRNA-miRNA-mRNA axis. In this case, circular RNA and mRNA may compete for the miRNA-response element, forming a natural competitive endogenous RNA network, according to Florian Karreth et al. [44]. In fact, only a few circRNAs have multiple binding sites, and only a few of these binding sites function for a particular miRNA [3]. The current study confirmed that only miR-136-5p, which was reported to be downregulated in different types of cancer and to participate as a tumor suppressor, could be functionally validated by both RNA pull-down and luciferase reporter assays among other potential targets [29, 45–48]. However, it is interesting that the expression of potential miRNA targets was high after pull-down but could not be validated by the luciferase reporter assay, suggesting that more underlying mechanisms are yet to be discovered. The Wnt/β-catenin pathway has been identified as a key pathway in carcinogenesis that can induce uncontrolled proliferation and migration, which

are quite common events in cancer [36, 49, 50]. As an essential member of the Wnt/β-catenin pathway, *WNT2* is reported to participate in several malignant tumors and is overexpressed in lesions of digestive tract cancers, including GC [32, 34–36, 49–53]. In our study, in vitro experiments confirmed that *WNT2* is the main conductor directly regulating proliferation, migration and invasion. In vivo, although overexpression of circOSBPL10 seemed to have little effect on tumor weight, tumor volume, and IF signals in mice injected with SGC-7901 cells, *WNT2* had a critical role in carcinogenesis in regulating tumor weight and size. Moreover, owing to the enhanced migration and invasion capability confirmed by cell experiments, in vivo imaging, and western blot, the epithelial–mesenchymal transition pathway might also be activated in addition to the Wnt/β-catenin pathway through overexpression of circOSBPL10, although this idea needs to be further explored. In addition, based on our results and previous outcomes, circular RNAs could serve as valuable prognostic factors owing to their stable expression and unique structure [17, 20]. However, we only detected the expression of circOSBPL10 in tumor tissues rather than in plasma samples from patients. Nonetheless, circulating circRNA may serve as a better prognostic marker in different diseases, as previously described [54, 55], although this point must be further confirmed.

In conclusion, we adopted several models and conducted functional experiments to confirm in vivo and in vitro that circOSBPL10 is upregulated in GC and can promote GC cell proliferation and migration by sponging miR-136-5p,

resulting in upregulated expression of *WNT2*. circOSBPL10 also serves as a valuable prognostic factor in GC. These findings suggest that circOSBPL10 could be a potential biomarker for diagnosis and a therapeutic target in GC.

Materials and methods

Patient samples

A total of 70 paired GC samples were collected from the Department of Gastric Surgery, the First Affiliated Hospital of Nanjing Medical University from 2012 to 2016. None of patients received preoperative chemotherapy. All specimens were snap-frozen in liquid nitrogen immediately after surgical resection. Clinicopathological features, which included gender, age, T stage, lymph node status, TNM stage (American Joint Committee on Cancer classification, AJCC) and tumor location, are shown in Table 1. The average follow-up time was 38.5 months (median 26.4 months; range 3-72 months). The follow-up interval was from the date of surgery to the date of disease progression, death or the last clinical investigation. This study was approved by The Clinical Research Ethics Committee of the First Affiliated Hospital of Nanjing Medical University. Written informed consent was obtained from all participants (approval no. IACUC-1711017).

RNA extraction

Total RNA samples from tumors and paired adjacent normal tissues were extracted separately using TRIzol reagent (Invitrogen, Carlsbad, CA, USA) according to the manufacturer's protocol. See Supplementary Methods.

Illumina-based RNA sequencing

Total RNA was first extracted with TRIzol reagent (Invitrogen, Carlsbad, CA, USA) and treated with DNase I to remove DNA contamination. Ribosome-depleted RNA was fragmented for cDNA synthesis with random hexamer primers. RNase H, dUTPs, buffer, and polymerase I were used for second-strand cDNA synthesis. The ligated double-stranded cDNA products were purified with magnetic beads and treated with uracil DNA glycosylase to remove the second-strand cDNA. Purified cDNA was subjected to PCR amplification for enrichment of the fragments, and strand-specific RNA-seq libraries were prepared for the Illumina system 2500.

Identification and quantification of circRNAs

This procedure was performed as previously described [17]. See Supplementary Methods.

PCR

Reverse transcription for circRNAs was implemented using Super-Script II (Takara, Dalian China) following the manufacturer's instructions. See Supplementary Methods.

Cell culture procedures

The human GC cell lines BGC-823 and SGC-7901 were cultured in RPMI1640 supplemented with 10% fetal bovine serum (FBS) and 1% penicillin-streptomycin. HEK-293T cells were cultured in Dulbecco's modified Eagle's medium supplemented with 10% FBS and 1% penicillin–streptomycin. All cells were cultured in a humidified 5% CO_2 incubator at 37 °C.

RNase R treatment

RNase R digestion was performed following previous protocols [19]. See Supplementary Methods.

Nuclear and cytoplasmic fractions

The nuclear and cytoplasmic fractions were extracted using NE-PER Nuclear and Cytoplasmic Extraction Reagents (Thermo Fisher Scientific, Waltham, MA, USA). Total RNA from lysates or the nuclear and cytoplasmic fractions were isolated using TRIzol (Invitrogen, Carlsbad, CA, USA).

Actinomycin D assay

BGC-823 cells were seeded at 5×10^4 cells per well in a 24-well plate overnight, and the total RNA was harvested at the indicated time points (4 h, 8 h, 12 h, 24 h) after treatment with 2 mg/L actinomycin D (Sigma-Aldrich, St. Louis, MO, USA). Then, qRT-PCR was performed to analyze the stability of the circRNA.

RNA FISH

FISH was performed using specific probes targeting the circOSBPL10 sequence. See Supplementary Methods.

Oligonucleotide transfection

siRNA, miRNA mimics and miRNA inhibitors were synthesized by RiboBio (Guangzhou, China). The cells were transfected using Lipofectamine 3000 (Thermo Fisher Scientific, Waltham, MA, USA) at a final concentration of 50 nM. At 48 h post transfection, cells were harvested for the assays described below. The detailed sequences are listed in Supplementary Table 1.

Cell proliferation, EdU, and colony formation assays

See Supplementary Methods.

Cell migration and invasion assay

A Transwell assay was performed to detect cell migration and invasion. See Supplementary Methods.

Western blot

Western blot was performed using the standard protocol. See Supplementary Methods.

xCELLigence real-time cell analysis of migration

Cell migration experiments were performed using an xCELLigence system with modified 16-well plates (Roche, Mannheim, Germany). According to the protocol, electrical signals from the indicated cells were monitored by sensors for over 24 h. The migratory activities of cells were evaluated by determining cell indexes.

Luciferase reporter assay

Luciferase assays were used to detect the binding of circRNA, miRNA, and mRNA. See Supplementary Methods.

miRNA prediction

miRNA target prediction was performed using the online databases starBase v2.0 (http://starbase.sysu.edu.cn), CircNet (http://circnet.mbc.nctu.edu.tw) and RNA22 (https://cm.jefferson.edu/rna22/).

circRNA overexpression construction and stable transfection

According to a previous protocol [56], to construct stable overexpression plasmids for circOSBPL10, cDNA was first synthesized and cloned into a pcDNA3.1 vector (Hanbio, Shanghai, China). A specially designed front circular frame and a back circular frame were obtained by PCR and then cloned into the pHB-CMV-MCS-EF1-copGFP-T2A-Puro vector at the EcoRI and BamHI sites. According to the manufacturer's guidelines, Lipofectamine 3000 (Life Technologies, Waltham, MA, USA) was used to transfect GC cell lines with this vector, and puromycin was used to filter cells with stable overexpression of circOSBPL10. The sequence was confirmed by sequencing. The circOSBPL10 overexpression plasmids were cloned into pHB-CMV-MCS-EF1-copGFP-T2A-Puro for lentiviral production (Hanbio,

Shanghai, China). HEK-293T cells were used for the production of lentiviruses as packaging cells. After HEK-293T cells reached a confluency of 70–80%, the circOSBPL10 overexpression plasmid combined with pSPAX2 and pMD2G packaging plasmids were used to transfect into the HEK-293T cells. After changing the media, the lentiviruses were collected for transduction into BGC-823 and MGC-803 cells for the in vivo experiments.

RNA pull-down assay

A pull-down assay was performed as previously described [19]. See Supplementary Methods.

Organoid culture

Organoid culture was performed as previously described [57]. See Supplementary Methods.

In vivo xenograft tumor model

A total of 50 Balb/c nude mice were purchased from Vital River (Beijing, China). Among them, 36 4-week-old mice were randomly divided into three groups, with 12 mice in each group. Either BGC-823 or SGC-7901 cells transfected with lenti-circOSBPL10-overexpression vectors were injected subcutaneously into the axilla of the forelimb (5×10^6 cells per mouse) of six mice in the lenti-circOSBPL10-overexpression (circOSBPL10) group. Ten days after subcutaneous injection, animal-specific cholesterol-modified siRNA obtained from RiboBio was injected twice a week for 2 weeks in the si-circOSBPL10 group, as previously reported [20, 58]. Negative control siRNA was injected twice a week for 2 weeks in the vector group. Tumor volumes were measured once a week. After 1 month, all mice were killed, and tumor weights and volumes were measured. The tumor volume was calculated as $V = \text{length} \times \text{width}^2 \times 0.5$. Immunofluorescence and immunohistochemistry were performed on tumor tissues, and quantification was performed in five random fields of view per section at $\times 600$ magnification and $\times 400$ magnification, respectively.

In vivo bioluminescence imaging

In vivo bioluminescence imaging was performed as previously described [59–61]. See Supplementary Methods.

IHC and IF analysis

IHC and IF analyses were performed as previously described [19, 21]. See Supplementary Methods.

Hematoxylin and eosin staining

Paraffin-embedded lung sections containing metastases were obtained from mice and stained with hematoxylin and eosin. Sections were cut into 5-μm slices for pathological evaluation and observation under a microscope (Olympus, Tokyo, Japan).

Statistical analysis

All statistical analyses were performed using SPSS 20.0 (IBM, SPSS, Chicago, IL, USA) and GraphPad Prism version 6.0 software; $P < 0.05$ was considered statistically significant. Student's t test and one-way analysis of variance were applied to compare continuous variables with a Gaussian distribution. DFS and OS curves were calculated using the Kaplan–Meier method and analyzed with the log-rank test.

Compliance with ethical standards

Conflict of interest The authors declare that they have no conflict of interest.

Publisher's note: Springer Nature remains neutral with regard to jurisdictional claims in published maps and institutional affiliations.

References

1. Allemani C, Weir HK, Carreira H, Harewood R, Spika D, Wang XS, et al. Global surveillance of cancer survival 1995-2009: analysis of individual data for 25,676,887 patients from 279 population-based registries in 67 countries (CONCORD-2). Lancet. 2015;385:977–1010.

2. Chen W, Zheng R, Baade PD, Zhang S, Zeng H, Bray F, et al. Cancer statistics in China, 2015. CA Cancer J Clin. 2016;66:115–32.

3. Chen W, Zheng R, Zhang S, Zeng H, Xia C, Zuo T, et al. Cancer incidence and mortality in China, 2013. Cancer Lett. 2017;401:63–71.

4. Torre LA, Bray F, Siegel RL, Ferlay J, Lortet-Tieulent J, Jemal A. Global cancer statistics, 2012. CA Cancer J Clin. 2015;65:87–108.

5. Oh SC, Sohn BH, Cheong JH, Kim SB, Lee JE, Park KC, et al. Clinical and genomic landscape of gastric cancer with a mesenchymal phenotype. Nat Commun. 2018;9:1777.

6. Zheng R, Zeng H, Zhang S, Chen T, Chen W. National estimates of cancer prevalence in China, 2011. Cancer Lett. 2016;370:33–38.

7. Ashwal-Fluss R, Meyer M, Pamudurti NR, Ivanov A, Bartok O, Hanan M, et al. circRNA biogenesis competes with pre-mRNA splicing. Mol Cell. 2014;56:55–66.

8. Li X, Liu CX, Xue W, Zhang Y, Jiang S, Yin QF, et al. Coordinated circRNA biogenesis and function with NF90/NF110 in viralinfection. Mol Cell. 2017;67:214–27. e217.

9. Memczak S, Jens M, Elefsinioti A, Torti F, Krueger J, Rybak A, et al. Circular RNAs are a large class of animal RNAs with regulatory potency. Nature. 2013;495:333–8.

10. Jeck WR, Sorrentino JA, Wang K, Slevin MK, Burd CE, Liu J, et al. Circular RNAs are abundant, conserved, and associated with ALU repeats. RNA. 2013;19:141–57.

11. Hentze MW, Preiss T. Circular RNAs: splicing's enigma variations. EMBO J. 2013;32:923–5.

12. Nigro JM, Cho KR, Fearon ER, Kern SE, Ruppert JM, Oliner JD, et al. Scrambled exons. Cell. 1991;64:607–13.

13. Abu N, Jamal R. Circular RNAs as promising biomarkers: a minireview. Front Physiol. 2016;7:355.

14. Liu J, Liu T, Wang X, He A. Circles reshaping the RNA world: from waste to treasure. Mol Cancer. 2017;16:58.

15. Salzman J, Gawad C, Wang PL, Lacayo N, Brown PO. Circular RNAs are the predominant transcript isoform from hundreds of human genes in diverse cell types. PLoS ONE. 2012;7:e30733.

16. Dong Y, He D, Peng Z, Peng W, Shi W, Wang J, et al. Circular RNAs in cancer: an emerging key player. J Hematol Oncol. 2017;10:2.

17. Chen J, Li Y, Zheng Q, Bao C, He J, Chen B, et al. Circular RNA profile identifies circPVT1 as a proliferative factor and prognostic marker in gastric cancer. Cancer Lett. 2017;388:208–19.

18. Zhong Z, Huang M, Lv M, He Y, Duan C, Zhang L, et al. Circular RNA MYLK as a competing endogenous RNA promotes bladder cancer progression through modulating VEGFA/VEGFR2 signaling pathway. Cancer Lett. 2017;403:305–17.

19. Li Y, Zheng F, Xiao X, Xie F, Tao D, Huang C, et al. CircHIPK3 sponges miR-558 to suppress heparanase expression in bladder cancer cells. EMBO Rep. 2017;18:1646–59.

20. Han D, Li J, Wang H, Su X, Hou J, Gu Y, et al. Circular RNA circMTO1 acts as the sponge of microRNA-9 to suppress hepatocellular carcinoma progression. Hepatology. 2017;66:1151–64.

21. Yao Z, Luo J, Hu K, Lin J, Huang H, Wang Q, et al. ZKSCAN1 gene and its related circular RNA (circZKSCAN1) both inhibit hepatocellular carcinoma cell growth, migration, and invasion but through different signaling pathways. Mol Oncol. 2017;11:422–37.

22. Zheng Q, Bao C, Guo W, Li S, Chen J, Chen B, et al. Circular RNA profiling reveals an abundant circHIPK3 that regulates cell growth by sponging multiple miRNAs. Nat Commun. 2016;7:11215.

23. Chen L, Zhang S, Wu J, Cui J, Zhong L, Zeng L, et al. circRNA_100290 plays a role in oral cancer by functioning as a sponge of the miR-29 family. Oncogene. 2017;36:4551–61.

24. Weng W, Wei Q, Toden S, Yoshida K, Nagasaka T, Fujiwara T, et al. Circular RNA ciRS-7-A promising prognostic biomarker and a potential therapeutic target in colorectal cancer. Clin Cancer Res. 2017;23:3918–28.

25. Burd CE, Jeck WR, Liu Y, Sanoff HK, Wang Z, Sharpless NE. Expression of linear and novel circular forms of an INK4/ARF-associated non-coding RNA correlates with atherosclerosis risk. PLoS Genet. 2010;6:e1001233.

26. Du WW, Yang W, Chen Y, Wu ZK, Foster FS, Yang Z, et al. Foxo3 circular RNA promotes cardiac senescence by modulating multiple factors associated with stress and senescence responses. Eur Heart J. 2017;38:1402–12.

27. Geng HH, Li R, Su YM, Xiao J, Pan M, Cai XX, et al. The circular RNA Cdr1as promotes myocardial infarction by

mediating the regulation of miR-7a on its target genes expression. PLoS ONE. 2016;11:e0151753.

28. Ferreira HJ, Davalos V, de Moura MC, Soler M, Perez-Salvia M, Bueno-Costa A, et al. Circular RNA CpG island hypermethylation-associated silencing in human cancer. Oncotarget. 2018;9:29208–19.

29. Li DX, Fei XR, Dong YF, Cheng CD, Yang Y, Deng XF, et al. The long non-coding RNA CRNDE acts as a ceRNA and promotes glioma malignancy by preventing miR-136-5p-mediated downregulation of Bcl-2 and Wnt2. Oncotarget. 2017;8:88163–78.

30. Cheng XX, Wang ZC, Chen XY, Sun Y, Kong QY, Liu J, et al. Frequent loss of membranous E-cadherin in gastric cancers: A cross-talk with Wnt in determining the fate of beta-catenin. Clin Exp Metastasis. 2005;22:85–93.

31. Cui J, Chen Y, Chou WC, Sun L, Chen L, Suo J, et al. An integrated transcriptomic and computational analysis for biomarker identification in gastric cancer. Nucleic Acids Res. 2011;39:1197–207.

32. Fu L, Zhang C, Zhang LY, Dong SS, Lu LH, Chen J, et al. Wnt2 secreted by tumour fibroblasts promotes tumour progression in oesophageal cancer by activation of the Wnt/beta-catenin signalling pathway. Gut. 2011;60:1635–43.

33. Huang L, Zhang KL, Li H, Chen XY, Kong QY, Sun Y, et al. Infrequent COX-2 expression due to promoter hypermethylation in gastric cancers in Dalian, China. Hum Pathol. 2006;37:1557–67.

34. Jung YS, Jun S, Lee SH, Sharma A, Park JI. Wnt2 complements Wnt/beta-catenin signaling in colorectal cancer. Oncotarget. 2015;6:37257–68.

35. Park JK, Song JH, He TC, Nam SW, Lee JY, Park WS. Overexpression of Wnt-2 in colorectal cancers. Neoplasma. 2009;56:119–23.

36. Qi J, Yu Y, Akilli Ozturk O, Holland JD, Besser D, Fritzmann J, et al. New Wnt/beta-catenin target genes promote experimental metastasis and migration of colorectal cancer cells through different signals. Gut. 2016;65:1690–701.

37. Hansen TB, Jensen TI, Clausen BH, Bramsen JB, Finsen B, Damgaard CK, et al. Natural RNA circles function as efficient microRNA sponges. Nature. 2013;495:384–8.

38. Dmitriev AA, Rosenberg EE, Krasnov GS, Gerashchenko GV, Gordiyuk VV, Pavlova TV, et al. Identification of novel epigenetic markers of prostate cancer by NotI-microarray sanalysis. Dis Markers. 2015;2015:241301.

39. Vater I, Montesinos-Rongen M, Schlesner M, Haake A, Purschke F, Sprute R, et al. The mutational pattern of primary lymphoma of the central nervous system determined by whole-exome sequencing. Leukemia. 2015;29:677–85.

40. Pongor L, Kormos M, Hatzis C, Pusztai L, Szabo A, Gyorffy B. A genome-wide approach to link genotype to clinical outcome by utilizing next generation sequencing and gene chip data of 6,697 breast cancer patients. Genome Med. 2015;7:104.

41. Meng S, Zhou H, Feng Z, Xu Z, Tang Y, Li P, et al. CircRNA: functions and properties of a novel potential biomarker for cancer. Mol Cancer. 2017;16:94.

42. Lu C, Shi X, Wang AY, Tao Y, Wang Z, Huang C, et al. RNA-Seq profiling of circular RNAs in human laryngeal squamous cell carcinomas. Mol Cancer. 2018;17:86.

43. Sierra B, Triska P, Soares P, Garcia G, Perez AB, Aguirre E, et al. OSBPL10, RXRA and lipid metabolism confer African-ancestry protection against dengue haemorrhagic fever in admixed Cubans. PLoS Pathog. 2017;13:e1006220.

44. Karreth FA, Pandolfi PP. ceRNA cross-talk in cancer: when cebling rivalries go awry. Cancer Discov. 2013;3:1113–21.

45. Chen P, Zhao L, Pan X, Jin L, Lin C, Xu W, et al. Tumor suppressor microRNA-136-5p regulates the cellular function of renal cell carcinoma. Oncol Lett. 2018;15:5995–6002.

46. Kristensen H, Thomsen AR, Haldrup C, Dyrskjot L, Hoyer S, Borre M, et al. Novel diagnostic and prognostic classifiers for prostate cancer identified by genome-wide microRNA profiling. Oncotarget. 2016;7:30760–71.

47. Singh A, Willems E, Singh A, Bin Hafeez B, Ong IM, Mehta SL, et al. Ultraviolet radiation-induced tumor necrosis factor alpha, which is linked to the development of cutaneous SCC, modulates differential epidermal microRNAs expression. Oncotarget. 2016;7:17945–56.

48. Ding H, Ye ZH, Wen DY, Huang XL, Zeng CM, Mo J, et al. Downregulation of miR-136-5p in hepatocellular carcinoma and its clinicopathological significance. Mol Med Rep. 2017;16:5393–405.

49. Kramer N, Schmollerl J, Unger C, Nivarthi H, Rudisch A, Unterleuthner D, et al. Autocrine WNT2 signaling in fibroblasts promotes colorectal cancer progression. Oncogene. 2017;36:5460–72.

50. Clevers H, Nusse R. Wnt/beta-catenin signaling and disease. Cell. 2012;149:1192–205.

51. Yuan H, Yu S, Cui Y, Men C, Yang D, Gao Z, et al. Knockdown of mediator subunit Med19 suppresses bladder cancer cell proliferation and migration by downregulating Wnt/beta-catenin signalling pathway. J Cell Mol Med. 2017;21:3254–63.

52. Zhou Y, Huang Y, Cao X, Xu J, Zhang L, Wang J, et al. WNT2 promotes cervical carcinoma metastasis and induction of epithelial-mesenchymal transition. PLoS ONE. 2016;11:e0160414.

53. Katoh M. WNT2 and human gastrointestinal cancer (review). Int J Mol Med. 2003;12:811–6.

54. Hang D, Zhou J, Qin N, Zhou W, Ma H, Jin G, et al. A novel plasma circular RNA circFARSA is a potential biomarker for non-small cell lung cancer. Cancer Med. 2018;7:2783–91.

55. Zhang J, Xu Y, Xu S, Liu Y, Yu L, Li Z, et al. Plasma circular RNAs, Hsa_circRNA_025016, predict postoperative atrial fibrillation after isolated off-pump coronary artery bypass grafting. J Am Heart Assoc. 2018;7:e006642.

56. Yang Y, Gao X, Zhang M, Yan S, Sun C, Xiao F, et al. Novel role of FBXW7 circular RNA in repressing glioma tumorigenesis. J Natl Cancer Inst. 2018;110:304–15.

57. Sun G-L, Li Z, Wang W-Z, Chen Z, Zhang L, Li Q, et al. miR-324-3p promotes gastric cancer development by activating Smad4-mediated Wnt/beta-catenin signaling pathway. J Gastroenterol. 2017;53:725–39.

58. Zhang F, Zhao L, Wang S, Yang J, Lu G, Luo N, et al. Construction of a biomimetic magnetosome and its application as a SiRNA carrier for high-performance anticancer therapy. Adv Funct Mater. 2018;28:1703326.

59. Wang N, Reeves KJ, Brown HK, Fowles AC, Docherty FE, Ottewell PD, et al. The frequency of osteolytic bone metastasis is determined by conditions of the soil, not the number of seeds; evidence from in vivo models of breast and prostate cancer. J Exp Clin Cancer Res. 2015;34:124.

60. Meleshina AV, Cherkasova EI, Shirmanova MV, Klementieva NV, Kiseleva EV, Snopova Lcapital Ve C, et al. Influence of mesenchymal stem cells on metastasis development in mice in vivo. Stem Cell Res Ther. 2015;6:15.

61. Sarkar TR, Battula VL, Werden SJ, Vijay GV, Ramirez-Pena EQ, Taube JH, et al. GD3 synthase regulates epithelial-mesenchymal transition and metastasis in breast cancer. Oncogene. 2015;34:2958–67.